ISSN 0915-633X

NATIONAL INSTITUTE FOR FUSION SCIENCE

Topics on MHD Equilibrium and Stability in Heliotron / Torsatron

K. Ichiguchi, N. Nakajima and M. Okamoto

(Received - Sep. 4, 1996)

NIFS-455 Oct. 1996

RESEARCH REPORT
NIFS Series

NAGOYA, JAPAN

Topics on MHD Equilibrium and Stability in Heliotron / Torsatron

Katsuji ICHIGUCHI, Noriyoshi NAKAJIMA, Masao OKAMOTO

National Institute for Fusion Science, Nagoya 464-01, Japan

Presented at 'Workshop on Theory of Fusion Plasmas', Varrenna, Aug.26-30, 1996.

Abstract

Recent topics on the MHD properties with and without bootstrap current in Heliotron / Torsatron configurations are presented.

In a currentless equilibrium with a large Shafranov shift, a high-n ballooning mode can be unstable even in the region with positive gradient of the rotational transform. This is because the local shear in the field line bending term can be reduced by the fact that the local enhancement of the poloidal field varies in the radial direction. Since the local curvature of the field lines depends on the label of the magnetic field line, α, in Heliotron/Torsatron, the eigenvalue ω^2 also depends on α. In the Mercier stable region, the level surfaces of ω^2 of unstable modes form spheroids in the (ψ, θ_k, α) space, where ψ and θ_k are the label of the flux surface and the radial wave number, while they form cylinders in tokamaks. Such high-n modes cannot be related to low-n modes in this case.

In the LHD configuration, bootstrap current depends on the collisionality of the plasma. When the beta value is raised by increasing the temperature with the density fixed, the plasma becomes less collisional and the bootstrap current grows in the direction where the rotational transform is increased. On the contrary, when the beta value is raised by increasing the density with the temperature fixed, the plasma becomes more collisional. While a small amount of the current flows in the same direction as in the above sequence at low beta in this case, the direction of the current reverses at high beta equilibrium. This is because the geometrical factor in the expression of the bootstrap current in the plateau regime has opposite signature to that in the $1/\nu$ regime. The latter equilibrium sequence is more stable in the Mercier criterion than the former one. Thus, the beta should be raised by increasing the density rather than the temperature to obtain stable high beta plasma.

Key Words ;

Heliotron/Torsatron, MHD, ballooning mode, Mercier criterion, local magnetic shear, bootstrap current, geometrical factor, collisionality of plasma.

1 Introduction

In this paper, we present the recent two topics on the MHD properties on Heliotron/Torsatron configurations.

The Heliotron/Torsatron configurations have an advantage that MHD equilibria can be achieved without net toroidal current. In the equilibria, pressure driven instability is crucial. Since there exist magnetic hill regions in such configurations, the stability against the interchange mode has been mainly studied. The ballooning mode, which is the other pressure driven mode, had been considered to be stable because the magnetic shear is positive, as speculated by Shafranov[1]. Recently, Cooper et al.[2] found unstable high-n ballooning modes in the positive $\iota'(\psi)$ region in three-dimensional (3D) equilibrium, where ι and ψ denote the rotational transform and the toroidal magnetic flux ; however, they did not give the reason. First, we consider the mechanism of the unstable high-n ballooning modes in the Heliotron/Torsatron configurations[3]. The degradation in the stabilizing contribution of the local shear is shown in high beta equilibria. The property in the stability of the ballooning modes is considered in both regions where the Mercier modes are stable and unstable.

On the other hand, the neoclassical theory shows that the bootstrap current can flow in the Heliotron/Torsatron plasmas[4, 5, 6, 7]. Thus, we consider the equilibria including the bootstrap current, secondly. Watanabe et al.[8, 9] calculated the bootstrap currents consistent with 3D MHD equilibria by utilizing the VMEC code[10]. They obtained substantial bootstrap currents which flow in the direction where the rotational transform is increased in the LHD plasma[11]. On the other hand, Ichiguchi et al.[12] found that the Mercier stability depends on the direction of the net toridal current with a profile peaked at the magnetic axis. The current flowing in the direction where the rotational transform is decreased has a stabilizing contribution, while the current in the direction where the rotational transform is increased has a destabilizing contribution. Therefore, the bootstrap current obtained by Watanabe et al. would destabilize the Mercier mode. The bootstrap current depends on the collisionality of the plasma in asymmetric configurations[5, 7]. Since the geometrical factor in the plateau regime has opposite sign to that in the $1/\nu$ regime, there is a possibility of the reverse in the direction of the bootstrap current. Thus, we consider the Mercier

stability of the 3D equilibria in the point of the direction of the bootstrap current[13].

2 Mechanism of High-n Ballooning Mode in Heliotron/Torsatron

The high-n ballooning mode equation for the incompressible perturbation ξ is given by

$$\boldsymbol{B}\cdot\nabla\left[\frac{|\boldsymbol{k}_\perp|^2}{B^2}\boldsymbol{B}\cdot\nabla\xi\right]+\frac{2}{B^4}\boldsymbol{B}\times\boldsymbol{k}_\perp\cdot\boldsymbol{\kappa}\boldsymbol{B}\times\boldsymbol{k}_\perp\cdot\nabla P\xi+\rho_m\omega^2\frac{|\boldsymbol{k}_\perp|^2}{B^2}\xi=0. \tag{2.1}$$

Here, $\boldsymbol{B}$, P, $\boldsymbol{\kappa}$ and ρ_m denote the magnetic field, the plasma pressure, the curvature of the field line and the mass density, respectively. $\boldsymbol{k}_\perp$ is the wave vector perpendicular to the magnetic field and ω^2 is the eigenvalue. Now, we employ the Boozer coordinates (ψ,θ,ζ)[14], where ψ is toroidal flux and θ and ζ are the poloidal and toroidal angle variables, respectively. It is convenient to consider Eq.(2.1) in the covering space, (ψ,η,α). Here, η is a coordinate in the direction of the field line, and α is a label of the field line on a flux surface, which are related with the Boozer coordinates as

$$\eta=\theta,\qquad \alpha=\zeta-\theta/\iota, \tag{2.2}$$

where ι denotes the rotational transform. The magnetic field in this space is given by $\boldsymbol{B}=\frac{1}{\iota}\nabla\alpha\times\nabla\psi$. The first term in eq.(2.1) corresponds to the field line bending, which has a stabilizing contribution to the ballooning mode. The second term is a driving term by the pressure gradient and the magnetic curvature. In Heliotron/Torsatron configurations, local structure of the magnetic field lines characterizes the behavior of the ballooning mode.

At first, we investigate the field line bending term in order to understand the existence of the unstable mode in the region with $\iota'(\psi)>0$. In this term, the normalized perpendicular wave vector under the currentless condition is given by

$$|\boldsymbol{k}_\perp|^2=\frac{2\psi}{B_0 g_{\theta\theta}}\left\{1+g_{\theta\theta}\left(\frac{|\nabla\psi|^2}{2\psi}\right)^2\left[\int^\eta\hat{s}d\eta\right]^2\right\}. \tag{2.3}$$

Here $\hat{s}$ is the local magnetic shear. In currentless equilibria, the integration of the local shear can be expressed by

$$\int^\eta\hat{s}d\eta=\bar{s}(\eta-\theta_k)+2\psi\frac{g_{\psi\theta}}{g_{\theta\theta}}, \tag{2.4}$$

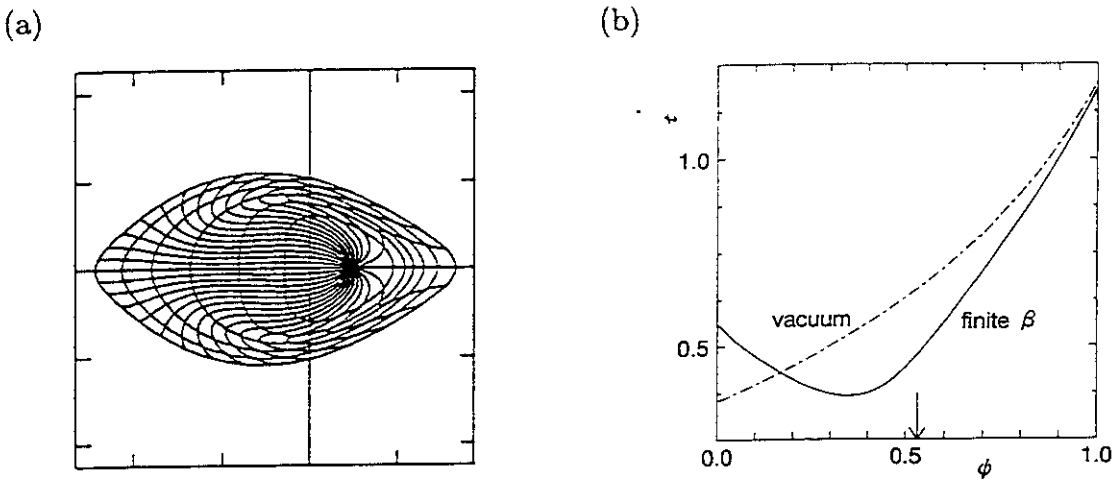

Fig.1 (a) (ψ, θ) grids of the Boozer coordinates in the cross section at $\zeta = const.$ and (b) profile of rotational transform of LHD plasma at $\beta_0 = 8\%$. The right side in (a) corresponds to the outside of the torus.

where θ_k denotes the radial wave number and $\bar{s}$ is the global magnetic shear defined by

$$\bar{s} = \frac{2\psi}{\iota} \frac{d\iota}{d\psi}, \tag{2.5}$$

and $g_{\psi\theta}$ and $g_{\theta\theta}$ are the covariant metrics in the Boozer coordinates.

Figure 1(a) shows a poloidal cross section with (ψ, θ) grids of a currentless LHD equilibrium at $\beta_0 = 8\%$, which is calculated with the VMEC code[10]. Here the pressure profile of $P = P_0(1 - \psi)^2$ is used. The sign of the metric $g_{\psi\theta}$ is related to the angle between the ψ-constant and θ-constant lines. In the equilibrium with large Shafranov shift as shown in Fig.1(a), sharp bends of the θ-constant lines can be seen in a flux surface in the outward region of the torus. We call the surface turning surface, where $g_{\psi\theta} = 0$. The turning surface roughly corresponds to the minimum point of the rotational transform in Fig.1(b). Inside the turning surface, $g_{\psi\theta}$ in the oscillatory part of the integrated local shear (the 2nd term of (2.4)) can be approximated as $c \sin\theta$ with positive c. In this region, the global magnetic shear $\bar{s}$ is negative. Thus, the integrated local magnetic shear given by eq.(2.4) is reduced as in tokamaks. On the other hand, outside the turning surface, where the global shear is positive, $g_{\psi\theta} \sim c \sin\theta$ with negative c. Therefore, the local magnetic shear can also be reduced even in the region with positive $\iota'(\psi)$, which leads to the substantial degradation of $|\boldsymbol{k}_\perp|^2$ around $\eta = \theta_k$ as shown in Fig.2 and the destabilization of High-n ballooning modes.

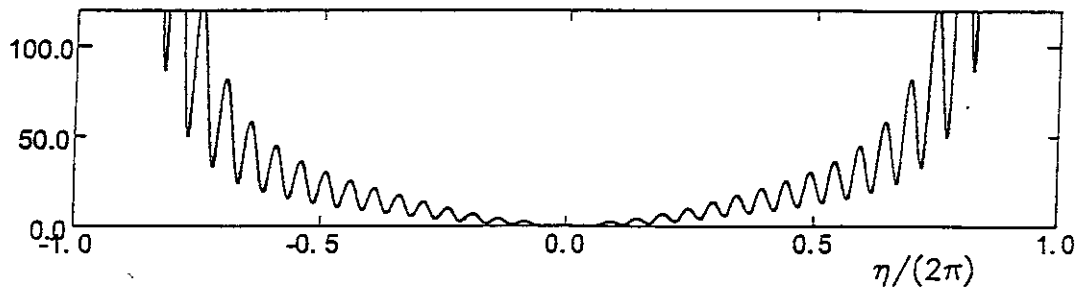

Fig.2 Profile of $|\boldsymbol{k}_\perp|^2$ along the field line with $\alpha = \theta_k = 0$ at the surface indicated by arrow in Fig.1(b).

These local properties of the magnetic field can be understood from the equilibrium force balance. In order to sustain the equilibrium with a large Shafranov shift, local enhancement of the poloidal field is needed in the outward region in the torus. In the vicinity of the magnetic axis, the average poloidal field decreases in the radial direction because of negative $\epsilon'(\psi)$. Hence, the enhancement of the local poloidal field increases in the radial direction, which corresponds to the enlargement of the distance of adjacent θ-constant lines. On the other hand, the average poloidal field radially increases in the peripheral region, because the property is inherently generated by the helical coils. Therefore, the local enhancement of the poloidal field decreases, and the distance between the θ-constant lines gets narrow. Thus, the turning surface appears around the local minimum point in the profile of the rotational transform.

In order to investigate the property of the high-n ballooning modes in Heliotron / Torsatron configurations, we consider the field line curvature of the second term in eq.(2.1) as well as the local shear. In tokamaks, the curvature is attributed to the toroidicity, and the field line has no α dependence. The local magnetic curvature in Heliotron/Torsatron equilibria consists of not only toroidal curvature but also helical curvature. This results in the fact that the local curvature is the most unfavorable at the outside region of the torus in the horizontally elongated cross section, while the curvature is locally favorable even at the outside region in the vertically elongated cross section. Thus, the local magnetic curvature outside of the torus strongly depends on the label of the field line, α.

Here we consider two types of the mode. One is the unstable mode in the Mercier stable region, which is shown in Fig.3(a). In this case, the high-n ballooning modes become unstable after the stabilizing effects of $|\boldsymbol{k}_\perp|^2$ is strongly modified to be reduced

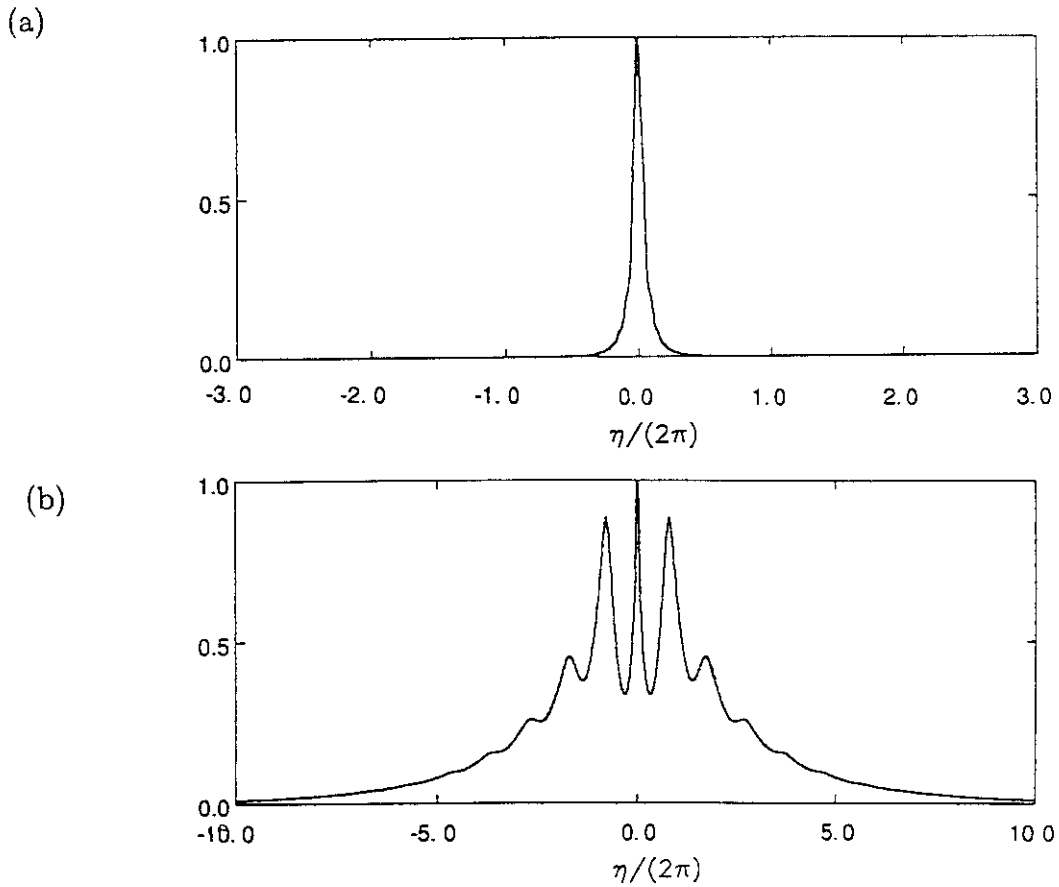

Fig.3 Eigenfunctions along the field line in (a) Mercier stable region corresponding to Fig.2 and (b) Mercier unstable region with weak α dependence.

sufficiently. The mode structure is strongly localized around $\eta = 0$ for $\theta_k = 0$ where the local magnetic shear is reduced, because the secular term in $|\boldsymbol{k}_\perp|^2$ is amplified by the large Shafranov shift through the factor of $|\nabla\psi|$ beyond $\eta = 2\pi$ as shown in Fig.2. Hence, the eigenvalue also strongly depends on α, i.e., $\omega^2 = \omega^2(\psi, \alpha, \theta_k)$. As shown in Fig.4, the topology of the level surfaces of unstable ω^2 is spheroid in the space of (ψ, α, θ_k), and the unstable region is surrounded by the level surface of stable TAE modes. Since the eigenvalue does not depend on α in tokamaks, i.e., $\omega^2 = \omega^2(\psi, \theta_k)$, the level surfaces are cylindrical and the method of quantum condition can be used to compose a global mode structure. It is difficult to apply the method to the spheroidal level surfaces because the toroidal mode number n is not a good quantum number. Even if it could be possible, the dominant number in n of the global modes would be much larger than the field period of the configuration, and therefore, the mode would be easily stabilized by kinetic effects, such as finite Larmor radius effect.

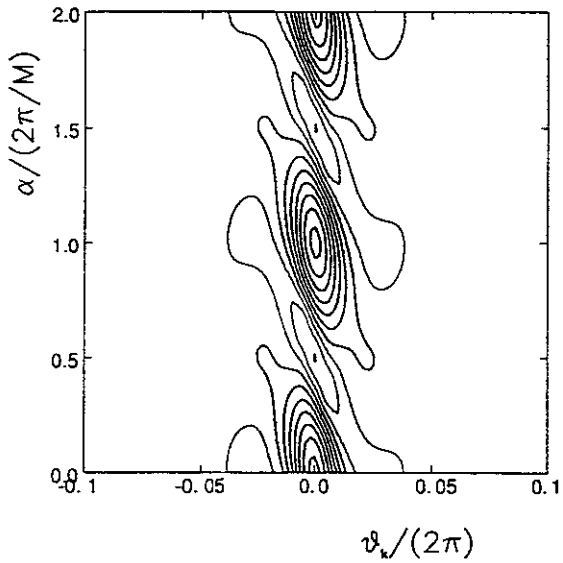

Fig.4 θ_k and α dependence of ω^2 at the surface indicated by arrow in Fig.1(b). Thick and thin lines show the contours of unstable high-n ballooning modes and stable TAE modes, respectively.

The other one is the unstable high-n ballooning mode in the Mercier unstable region. We study the mode in the equilibrium with a broad pressure profile of $P = P_0(1-\psi^2)^2$. In the Mercier unstable region, the high-n ballooning modes become unstable where the $|\boldsymbol{k}_\perp|^2$ is not so much modified as that in the above Mercier stable equilibria. Hence, not only the modes strongly localized in the region with the unfavorable local curvature, but also the modes with extended structure along the field line can be destabilized by the unfavorable averaged curvature in the region as shown in Fig.3(b).

The latter modes have smaller eigenvalues than those in the former modes, because the eigenfunction passes both the unfavorable and the favorable local curvature regions. Thus, the dependence of the eigenvalues of the latter modes on α is weak, while the eigenvalues in the former modes strongly depend on α. Hence, the level surface of small ω^2 corresponding to the extended mode structure would be continuous in α direction, or nearly cylindrical, in the (ψ, θ_k, α) space, and the spheroidal structures with large ω^2 corresponding to the strongly localized mode structure exist inside the continuous surface.

3 Stability of High Beta Equilibria Carrying Bootstrap Currents

We calculated the 3D MHD equilibria consistent with the bootstrap current by iterating the equilibrium calculation with the VMEC code[10] and the evaluation of the bootstrap current. In the calculations, we assumed that the plasma is composed

of only electrons and protons and they have the same temperature, T, and the density n, which are given by

$$T(\psi) = T_0(1-\psi), \qquad n(\psi) = n_0(1-\psi). \tag{3.1}$$

In this case, the bootstrap current in each limits of the $1/\nu$ and the plateau regimes is expressed as

$$I_b(\psi) = 2\pi \int d\psi \frac{\langle \boldsymbol{J}_b \cdot \boldsymbol{B} \rangle}{\langle \boldsymbol{B}^2 \rangle}, \tag{3.2}$$

$$\langle \boldsymbol{J}_b \cdot \boldsymbol{B} \rangle = -G_b \left[L_1 \frac{dP}{d\psi} + L_2 n \frac{dT}{d\psi} \right], \tag{3.3}$$

where the brackets denote the surface average and $L_j (j = 1, 2)$ are transport coefficients which include the viscosity and the friction coefficients[7].

Here, G_b is called geometrical factor, which determines the direction of the neoclassical flow damping caused by the viscosity. The geometrical factor in asymmetric configuration depends on the magnetic structure of the configuration and the collisionality of the particle, because it reflects the property of the orbits of the particles. Since the bootstrap current flows in the direction where the neoclassical flow would not damp, it can reverse the direction when the damping direction changes depending on the geometrical factor. The expressions of the geometrical factor in the Boozer coordinates in the limits of the $1/\nu$ regime, $G_b^{1/\nu}$, and the plateau regime, G_b^{pl} are given in Refs.[7] and [9], respectively. In order to evaluate the bootstrap current continuously between the $1/\nu$ and the plateau regimes, a connection formula in Ref.[9] is utilized. Since we assume that the electrons and the ions have the same T and n, the contribution of the radial electric field to the bootstrap current[15] vanishes in eq.(3.3).

We consider two sequences of equilibria in raising the beta value in the LHD configuration [11]. One is the temperature sequence where the temperature is increased with the density fixed at $n_0 = 0.2 \times 10^{20} m^{-3}$. The other one is the density sequence where the density is increased with the temperature fixed at $T_0 = 0.5 keV$. We also assumed $B_0 = 1T$.

The total bootstrap currents given by (3.2) in the two sequences are shown in Fig.5. The positive value in the figure corresponds to the net toroidal current flowing in the direction where the rotational transform is increased. In the temperature sequence,

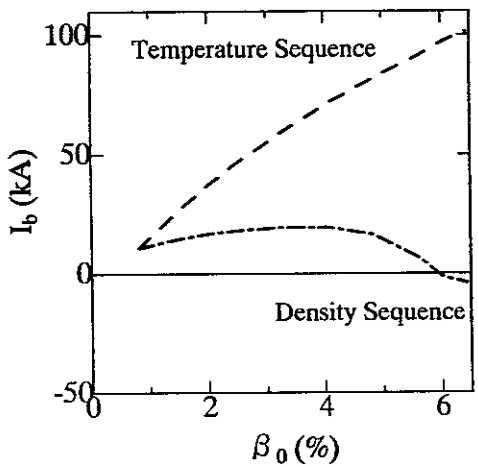

Fig.5 Total bootstrap currents versus β_0 in the temperature sequence (dashed line) and the density sequence (dot-dashed line).

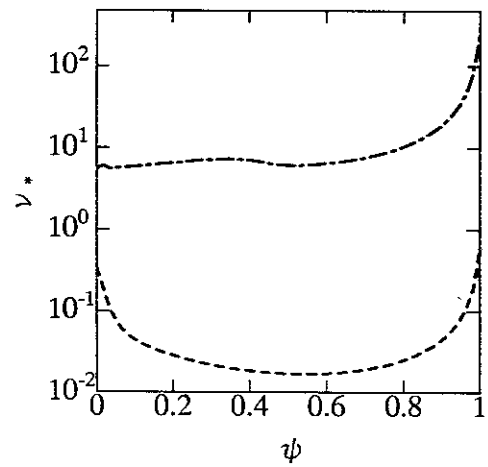

Fig.6 Profiles of normalized collision frequency. Dashed and dot-dashed lines show the values at $\beta_0 = 6.4\%$ in the temperature and the density sequences, respectively.

the positive bootstrap current is enhanced as the beta value grows. On the other hand, in the density sequence, the total bootstrap current is enhanced in the positive direction up to $\beta_0 = 4\%$, where β_0 is the beta value at the magnetic axis; however the absolute value is much less than that in the temperature sequence. The current is reduced beyond $\beta_0 = 4\%$ and becomes negative for $\beta_0 \geq 6\%$. That is, the total bootstrap current reverses the direction.

In order to know the collisionality of equilibria in the two sequences, we plotted the normalized collision frequency by the averaged bounce frequency of the banana orbit, ν_*[9], in Fig.6. In the temperature sequence, the plasma becomes less collisional as beta grows. The collisionality of the plasma at $\beta_0 = 6.4\%$ ($T_0 = 4keV$) almost enters the $1/\nu$ regime because $\nu_* << 1$. Therefore, the geometrical factor is almost determined by $G_b^{1/\nu}$. As shown in Fig.7, where the geometrical factors normalized by that in the equivalent tokamak, J/ι are plotted, $G_b^{1/\nu}$ has large positive value in the whole plasma region and the profile is insensitive to the beta value. Thus, the large positive bootstrap current is attributed to this property of $G_b^{1/\nu}$.

On the other hand, the plasma becomes more collisional as beta grows in the density sequence, and the plasma is close to the plateau regime at $\beta_0 = 6.4\%$ ($n_0 = 1.6 \times$

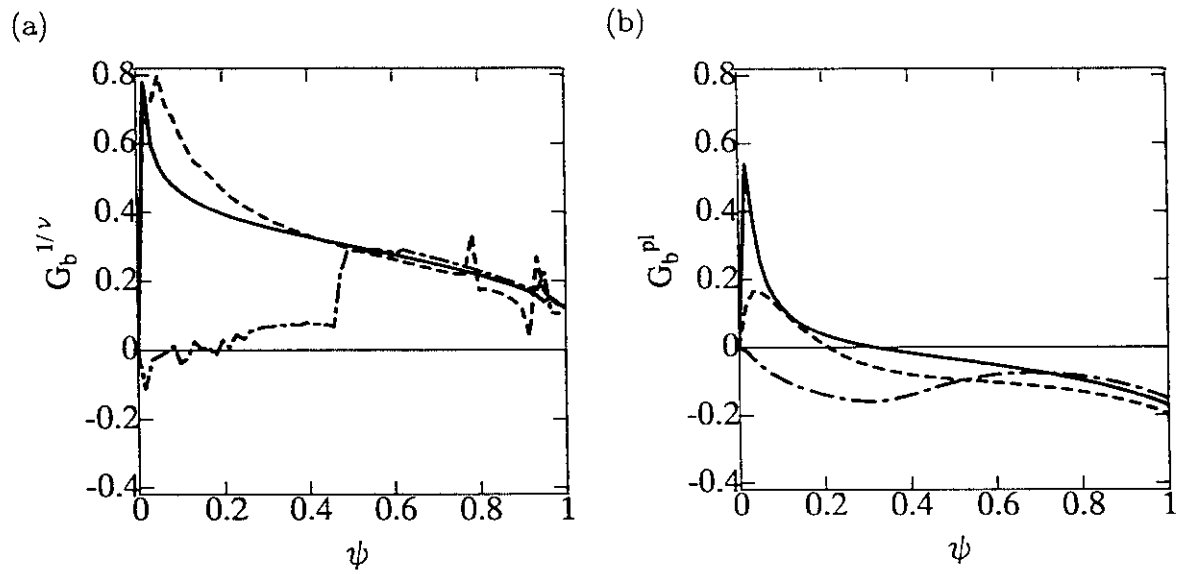

Fig.7 Profiles of normalized geometrical factors in the limit of (a) $1/\nu$ and (b) plateau regimes with $B_0 = 1T$. Solid lines show the values in the vacuum configuration. Dashed and dot-dashed lines correspond to the same lines in Fig.6, respectively.

$10^{20}m^{-3}$) because $\nu_* > 1$ in Fig.6. Hence, the contribution of G_b^{pl} in the geometrical factor becomes dominant, which has the negative value in the whole plasma region at the beta value, as shown in Fig.7. Thus, the reverse in the direction of the total bootstrap current occurs mainly due to the contribution of negative G_b^{pl} . However, the bootstrap current density only partially reverses the direction and there exists a small region with positive current density. A substantial reduction of $G_b^{1/\nu}$ is seen in the central region corresponding to the negative current density. Therefore, the change of the profile in $G_b^{1/\nu}$ also advances the reverse.

Figure 8 shows the profiles of the rotational transform in the two sequences. The rotational transform can be divided as follow:

$$\iota = \iota_{vac} + \iota_{BS} + \iota_{PS}, \tag{3.4}$$

where ι_{vac} denotes the rotational transform generated by the vacuum magnetic field and ι_{BS} and ι_{PS} are the contributions from the bootstrap current and the diamagnetic effects attributed to the Pfirsch-Schlüter current. The last term is sensitive to the sum of others. At $\beta_0 = 6.4\%$, ι_{BS} is positive in the temperature sequence, while it is negative in the density sequence. Thus, the sum of the first two terms in eq.(3.4) increases and decreases in the temperature and the density sequences, respectively. Since the bootstrap current can be treated as a given additional net toroidal current,

the Shafranov shift is considered to be proportional to the inverse of the square of the sum of the first two terms in the large aspect ratio limit. Hence, the Shafranov shift is enhanced in the density sequence. The large Shafranov shift enhances the magnetic well. As is seen in the currentless equilibria in Fig.1(b), the deformation of the flux surfaces accompanied with the Shafranov shift brings the increase of ι_{PS} at the magnetic axis and the decrease at the peripheral region so as to produce a local minimum in the profile. Therefore, the magnetic shear is enhanced in the peripheral region. On the contrary, the contribution of ι_{PS} is small in eq.(3.4) the Shafranov shift is suppressed because of the positive ι_{BS} in the temperature sequence.

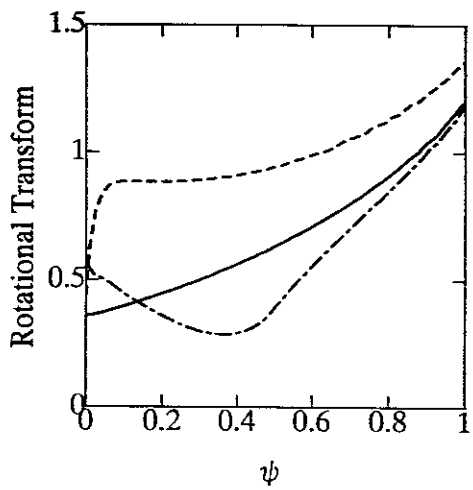

Fig.8 Rotational transform profiles. Solid, dashed and dot-dashed lines correspond to the the same lines in Fig.7, respectively.

As a result, in the density sequence, both enhancements of the magnetic well and the magnetic shear stabilize the Mercier mode owing to the decrease in the rotational transform by the bootstrap current. Figure 9 shows the Mercier unstable region and the contours of D_I[16], which is the normalized Mercier criterion so that the shear term should be $-1/4$. An unstable region is seen in the density sequence in Fig.9(b). However, the value of D_I is small and the lines indicating the positions of resonant surfaces of low mode-number global modes almost avoid the region with $D_I > 0.2$. Because the global modes can often be seen over $D_I \simeq 0.2$[17], there would not exist an unstable global mode degrading the confinement drastically although some fluctuations may be observed. Furthermore, the second stability region for the Mercier criterion appears beyond $\beta_0 = 5.8\%$ which is lower than that in the corresponding currentless equilibrium sequence[12]. This is because the local bootstrap current already flows in the negative direction in the central region of the plasma even in the equilibria where the total bootstrap current is zero.

On the other hand, in the temperature sequence, there exists a large unstable region

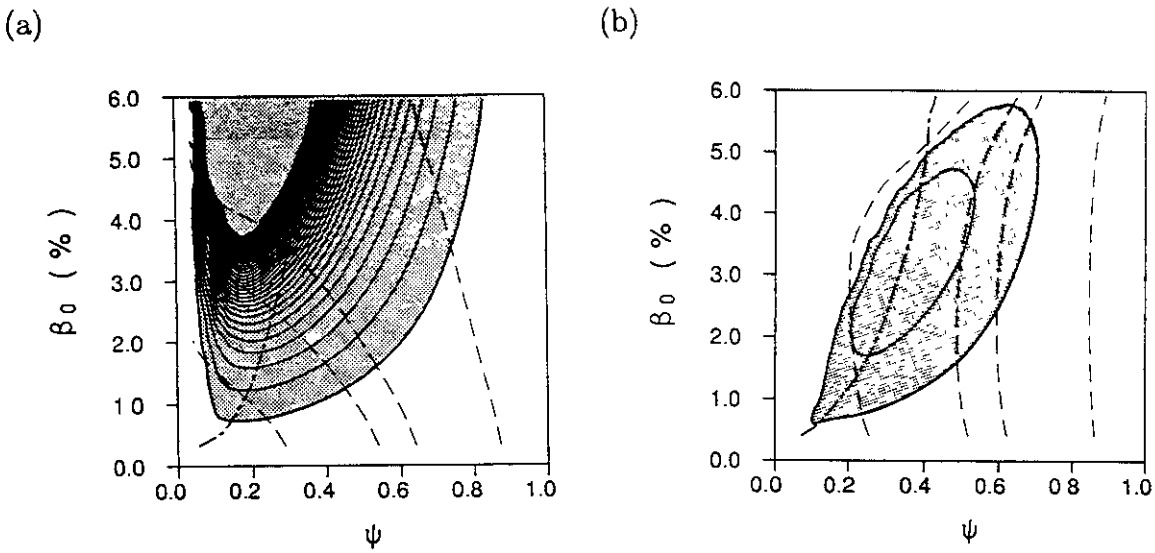

Fig.9 Mercier unstable regions for (a) temperature sequence and (b) density sequence in the (β_0, ψ) plane. Shaded regions show unstable regions. Solid lines in these regions are the contours of the level surface of D_I which differ by $\Delta D_I = 0.2$. In (a) the contours with $D_I > 8.0$ are not plotted because they are too dense. Dot-dashed line shows the boundary between the magnetic well and hill regions. Dashed lines indicate the positions of the rational surfaces corresponding to $\iota = 1,\ 3/4,\ 2/3$ and $1/2$ from right to left.

in the plasma column in Fig.9(a) and the value of D_I is enhanced as the beta value grows. Therefore, a considerable unstable global mode will appear even in low beta equilibria. This is because the magnetic well and the magnetic shear are suppressed due to the small Shafranov shift.

In equilibria with net toroidal currents, current driven mode is also suspicious ; however, the unstable internal kink mode is not found in either sequence. The rotational transform must monotonically and weakly decrease from the magnetic axis to the resonant surface in order for the internal kink mode to be destabilized in Heliotron / Torsatron [18]. ι' is positive around the magnetic axis in the temperature sequence, and the shear can be negative but too strong there in the density sequence.

4 Summary

Here we presented the topics on the properties of high-n ballooning mode and the collisionality dependence of the MHD stability through the change in the bootstrap current in Heliotron/Torsatron.

The reason why the high-n mode can be unstable in the region with positive $\iota'(\psi)$

can be understood by considering the reduction of the local magnetic shear in the equilibrium with a large Shafranov shift. In order to maintain the force balance, local poloidal magnetic field is necessarily enhanced in the outside of the torus. The enhanced poloidal field decreases in the radial direction in the region with positive $\epsilon'(\psi)$. Thus, the oscillatory part can cancel the secular part around $\eta = \theta_k$ in the local magnetic shear. Consequently, the stabilizing effect in the field line bending term is substantially reduced.

The high-n ballooning mode is driven by the local magnetic curvature. In the Mercier stable region, the mode structure is strongly localized along the field line where the local curvature is unfavorable because the weak local shear region is narrow. Since the local curvature depends on the label of the field line, α, the mode structure and the eigenvalue also strongly depend on α, i.e., $\omega^2 = \omega^2(\psi, \theta_k, \alpha)$. This point is quite different from that in tokamaks where the eigenvalue does not depend on α i.e., $\omega^2 = \omega^2(\psi, \theta_k)$. Therefore, the level surfaces of the eigenvalue are like spheroid in the (ψ, θ_k, α) space, while those in tokamaks are like cylinder. In this case, the high-n mode cannot be connected to low-n modes. In the Mercier unstable region, there exist continuous level surfaces of the eigenvalue in α direction outside the spheroids. The mode structure corresponding to the continuous level surface is fairly extended along the field line and is driven by the average magnetic curvature.

The geometrical factor in the expression of the bootstrap current which plays a dominant role has different dependence on the collisionality in Heliotron/Torsatron configuration. Here we considered two cases of the temperature and the density sequences in raising the beta value to investigate the collisionality dependence of the equilibria with the bootstrap currents.

In the temperature sequence, we raised the beta value by increasing the temperature with the density fixed. Then, the plasma becomes less collisional as beta grows, and the geometrical factor is dominated by $G_b^{1/\nu}$. The signature of $G_b^{1/\nu}$ is still positive in high beta equilibria. We obtained a significant bootstrap current flowing in the direction where the rotational transform is increased. In the density sequence, we raised the beta value by increasing the density with the fixed temperature. In this sequence, the plasma approaches to the plateau regime. In the geometrical factor in

the connection formula, the contribution of G_b^{pl} becomes dominant. G_b^{pl} has opposite signature to that of $G_b^{1/\nu}$ in LHD. Hence, the total bootstrap current reverses the direction and flows in the direction where the rotational transform is decreased at last. In this case, the reduction of the positive $G_b^{1/\nu}$ in the central region advances the reverse of the bootstrap current as well as the enhancement of the contribution of negative G_b^{pl}.

In the equilibrium in the density sequence, the enlarged Shafranov shift by the reduction of the rotational transform enhances the stabilizing effects of the magnetic shear and the magnetic well. Therefore, the Mercier stability is improved and a second stability region appears at lower beta value than that in the corresponding currentless equilibrium sequence. On the contrary, the Mercier stability in the equilibrium in the temperature sequence is deteriorated because of the suppression of the Shafranov shift. Thus, the beta value should be raised by increasing the density rather than the temperature to obtain a stable plasma in high-beta experiments in LHD.

References

[1] V.D.Shafranov, Phys. Fluids **26** (1983) 357.

[2] W.A.Cooper, S.P.Hirshman, D.K.Lee, Nucl. Fusion **29** (1989) 617.

[3] N.Nakajima, (submitted to Phys. Plasmas)

[4] K.C.Shaing, J.D.Callen, Phys. Fluids **26** (1983) 3315.

[5] K.C.Shaing, et al., Phys. Fluids **B1** (1989) 1663.

[6] N.Nakajima, et al., Nucl. Fusion **29** (1989) 605.

[7] N.Nakajima, M.Okamoto, J. Phys. Soc. Jpn. **61** (1992) 833.

[8] K.Watanabe, et al., Nucl. Fusion **32** (1992) 1499.

[9] K.Watanabe, et al., Nucl. Fusion **35** (1995) 335.

[10] S.P.Hirshman, W.I. Van Rij, P.Merkel, Comp. Phys. Comm. **43** (1986) 143.

[11] A.Iiyoshi, et al., Fusion Tech. **17** (1990) 169.

[12] K.Ichiguchi, et al., Nucl. Fusion **33** (1993) 481.

[13] K.Ichiguchi, Proc. Australia-Japan Plasma Theory Workshop 1995 at Robertson, (1996) 35.

[14] A.H.Boozer, Phys. Fluids **25** (1982) 520.

[15] N.Nakajima, M.Okamoto, M.Fujiwara, Kakuyugo Kenkyu, **68** (1992) 503.

[16] A.H.Glasser, J.M.Greene, J.L.Johnson, Phys. Fluids **18** (1975) 875.

[17] Y.Nakamura, K.Ichiguchi, et al., J. Phys. Soc. Jpn. **58** (1989) 3157.

[18] K.Ichiguchi, (in preparation for publication).

Recent Issues of NIFS Series

NIFS-418 J. Uramoto,
Extraction of K^- Mesonlike Particles from a D_2 Gas Discharge Plasma in Magnetic Field; May 1996

NIFS-419 J. Xu, K. Toi, H. Kuramoto, A. Nishizawa, J. Fujita, A. Ejiri, K. Narihara, T. Seki, H. Sakakita, K. Kawahata, K. Ida, K. Adachi, R. Akiyama, Y. Hamada, S. Hirokura, Y. Kawasumi, M. Kojima, I. Nomura, S. Ohdachi, K.N. Sato
Measurement of Internal Magnetic Field with Motional Stark Polarimetry in Current Ramp-Up Experiments of JIPP T-IIU; June 1996

NIFS-420 Y.N. Nejoh,
Arbitrary Amplitude Ion-acoustic Waves in a Relativistic Electron-beam Plasma System; July 1996

NIFS-421 K. Kondo, K. Ida, C. Christou, V.Yu.Sergeev, K.V.Khlopenkov, S.Sudo, F. Sano, H. Zushi, T. Mizuuchi, S. Besshou, H. Okada, K. Nagasaki, K. Sakamoto, Y. Kurimoto, H. Funaba, T. Hamada, T. Kinoshita, S. Kado, Y. Kanda, T. Okamoto, M. Wakatani and T. Obiki,
Behavior of Pellet Injected Li Ions into Heliotron E Plasmas; July 1996

NIFS-422 Y. Kondoh, M. Yamaguchi and K. Yokozuka,
Simulations of Toroidal Current Drive without External Magnetic Helicity Injection; July 1996

NIFS-423 Joong-San Koog,
Development of an Imaging VUV Monochromator in Normal Incidence Region; July 1996

NIFS-424 K. Orito,
A New Technique Based on the Transformation of Variables for Nonlinear Drift and Rossby Vortices; July 1996

NIFS-425 A. Fujisawa, H. Iguchi, S. Lee, T.P. Crowley, Y. Hamada, H. Sanuki, K. Itoh, S. Kubo, H. Idei, T. Minami, K. Tanaka, K. Ida, S. Nishimura, S. Hidekuma, M. Kojima, C. Takahashi, S. Okamura and K. Matsuoka,
Direct Observation of Potential Profiles with a 200keV Heavy Ion Beam Probe and Evaluation of Loss Cone Structure in Toroidal Helical Plasmas on the Compact Helical System; July 1996

NIFS-426 H. Kitauchi, K. Araki and S. Kida,
Flow Structure of Thermal Convection in a Rotating Spherical Shell; July 1996

NIFS-427 S. Kida and S. Goto,
Lagrangian Direct-interaction Approximation for Homogeneous Isotropic

Turbulence; July 1996

NIFS-428 V.Yu. Sergeev, K.V. Khlopenkov, B.V. Kuteev, S. Sudo, K. Kondo, F. Sano, H. Zushi, H. Okada, S. Besshou, T. Mizuuchi, K. Nagasaki, Y. Kurimoto and T. Obiki,
Recent Experiments on Li Pellet Injection into Heliotron E; Aug. 1996

NIFS-429 N. Noda, V. Philipps and R. Neu,
A Review of Recent Experiments on W and High Z Materials as Plasma-Facing Components in Magnetic Fusion Devices; Aug. 1996

NIFS-430 R.L. Tobler, A. Nishimura and J. Yamamoto,
Design-Relevant Mechanical Properties of 316-Type Stainless Steels for Superconducting Magnets; Aug. 1996

NIFS-431 K. Tsuzuki, M. Natsir, N. Inoue, A. Sagara, N. Noda, O. Motojima, T. Mochizuki, T. Hino and T. Yamashina,
Hydrogen Absorption Behavior into Boron Films by Glow Discharges in Hydrogen and Helium; Aug. 1996

NIFS-432 T.-H. Watanabe, T. Sato and T. Hayashi,
Magnetohydrodynamic Simulation on Co- and Counter-helicity Merging of Spheromaks and Driven Magnetic Reconnection; Aug. 1996

NIFS-433 R. Horiuchi and T. Sato,
Particle Simulation Study of Collisionless Driven Reconnection in a Sheared Magnetic Field; Aug. 1996

NIFS-434 Y. Suzuki, K. Kusano and K. Nishikawa,
Three-Dimensional Simulation Study of the Magnetohydrodynamic Relaxation Process in the Solar Corona. II.; Aug. 1996

NIFS-435 H. Sugama and W. Horton,
Transport Processes and Entropy Production in Toroidally Rotating Plasmas with Electrostatic Turbulence; Aug. 1996

NIFS-436 T. Kato, E. Rachlew-Källne, P. Hörling and K.-D Zastrow,
Observations and Modelling of Line Intensity Ratios of OV Multiplet Lines for 2s3s 3S1 - 2s3p 3Pj; Aug. 1996

NIFS-437 T. Morisaki, A. Komori, R. Akiyama, H. Idei, H. Iguchi, N. Inoue, Y. Kawai, S. Kubo, S. Masuzaki, K. Matsuoka, T. Minami, S. Morita, N. Noda, N. Ohyabu, S. Okamura, M. Osakabe, H. Suzuki, K. Tanaka, C. Takahashi, H. Yamada, I. Yamada and O. Motojima,
Experimental Study of Edge Plasma Structure in Various Discharges on Compact Helical System; Aug. 1996

NIFS-438 A. Komori, N. Ohyabu, S. Masuzaki, T. Morisaki, H. Suzuki, C. Takahashi, S. Sakakibara, K. Watanabe, T. Watanabe, T. Minami, S. Morita, K. Tanaka, S.

Ohdachi, S. Kubo, N. Inoue, H. Yamada, K. Nishimura, S. Okamura, K. Matsuoka, O. Motojima, M. Fujiwara, A. Iiyoshi, C. C. Klepper, J.F. Lyon, A.C. England, D.E. Greenwood, D.K. Lee, D.R. Overbey, J.A. Rome, D.E. Schechter and C.T. Wilson,
Edge Plasma Control by a Local Island Divertor in the Compact Helical System; Sep. 1996 (IAEA-CN-64/C1-2)

NIFS-439 K. Ida, K. Kondo, K. Nagaski T. Hamada, H. Zushi, S. Hidekuma, F. Sano, T. Mizuuchi, H. Okada, S. Besshou, H. Funaba, Y. Kurimoto, K. Watanabe and T. Obiki,
Dynamics of Ion Temperature in Heliotron-E; Sep. 1996 (IAEA-CN-64/CP-5)

NIFS-440 S. Morita, H. Idei, H. Iguchi, S. Kubo, K. Matsuoka, T. Minami, S. Okamura, T. Ozaki, K. Tanaka, K. Toi, R. Akiyama, A. Ejiri, A. Fujisawa, M. Fujiwara, M. Goto, K. Ida, N. Inoue, A. Komori, R. Kumazawa, S. Masuzaki, T. Morisaki, S. Muto, K. Narihara, K. Nishimura, I. Nomura, S. Ohdachi, M.. Osakabe, A. Sagara, Y. Shirai, H. Suzuki, C. Takahashi, K. Tsumori, T. Watari, H. Yamada and I. Yamada,
A Study on Density Profile and Density Limit of NBI Plasmas in CHS; Sep. 1996 (IAEA-CN-64/CP-3)

NIFS-441 O. Kaneko, Y. Takeiri, K. Tsumori, Y. Oka, M. Osakabe, R. Akiyama, T. Kawamoto, E. Asano and T. Kuroda,
Development of Negative-Ion-Based Neutral Beam Injector for the Large Helical Device; Sep. 1996 (IAEA-CN-64/GP-9)

NIFS-442 K. Toi, K.N. Sato, Y. Hamada, S. Ohdachi, H. Sakakita, A. Nishizawa, A. Ejiri, K. Narihara, H. Kuramoto, Y. Kawasumi, S. Kubo, T. Seki, K. Kitachi, J. Xu, K. Ida, K. Kawahata, I. Nomura, K. Adachi, R. Akiyama, A. Fujisawa, J. Fujita, N. Hiraki, S. Hidekuma, S. Hirokura, H. Idei, T. Ido, H. Iguchi, K. Iwasaki, M. Isobe, O. Kaneko, Y. Kano, M. Kojima, J. Koog, R. Kumazawa, T. Kuroda, J. Li, R. Liang, T. Minami, S. Morita, K. Ohkubo, Y. Oka, S. Okajima, M. Osakabe, Y. Sakawa, M. Sasao, K. Sato, T. Shimpo, T. Shoji, H. Sugai, T. Watari, I. Yamada and K. Yamauti,
Studies of Perturbative Plasma Transport, Ice Pellet Ablation and Sawtooth Phenomena in the JIPP T-IIU Tokamak; Sep. 1996 (IAEA-CN-64/A6-5)

NIFS-443 Y. Todo, T. Sato and The Complexity Simulation Group,
Vlasov-MHD and Particle-MHD Simulations of the Toroidal Alfvén Eigenmode; Sep. 1996 (IAEA-CN-64/D2-3)

NIFS-444 A. Fujisawa, S. Kubo, H. Iguchi, H. Idei, T. Minami, H. Sanuki, K. Itoh, S. Okamura, K. Matsuoka, K. Tanaka, S. Lee, M. Kojima, T.P. Crowley, Y. Hamada, M. Iwase, H. Nagasaki, H. Suzuki, N. Inoue, R. Akiyama, M. Osakabe, S. Morita, C. Takahashi, S. Muto, A. Ejiri, K. Ida, S. Nishimura, K. Narihara, I. Yamada, K. Toi, S. Ohdachi, T. Ozaki, A. Komori, K. Nishimura, S. Hidekuma, K. Ohkubo, D.A. Rasmussen, J.B. Wilgen, M. Murakami, T. Watari and M. Fujiwara,
An Experimental Study of Plasma Confinement and Heating Efficiency

through the Potential Profile Measurements with a Heavy Ion Beam Probe in the Compact Helical System; Sep. 1996 (IAEA-CN-64/C1-5)

NIFS-445 O. Motojima, N. Yanagi, S. Imagawa, K. Takahata, S. Yamada, A. Iwamoto, H. Chikaraishi, S. Kitagawa, R. Maekawa, S. Masuzaki, T. Mito, T. Morisaki, A. Nishimura, S. Sakakibara, S. Satoh, T. Satow, H. Tamura, S. Tanahashi, K. Watanabe, S. Yamaguchi, J. Yamamoto, M.Fujiwara and A. Iiyoshi,
Superconducting Magnet Design and Construction of LHD; Sep. 1996 (IAEA-CN-64/G2-4)

NIFS-446 S. Murakami, N. Nakajima, S. Okamura, M. Okamoto and U. Gasparino,
Orbit Effects of Energetic Particles on the Reachable β–Value and the Radial Electric Field in NBI and ECR Heated Heliotron Plasmas; Sep. 1996 (IAEA-CN-64/CP -6) Sep. 1996

NIFS-447 K. Yamazaki, A. Sagara, O. Motojima, M. Fujiwara, T. Amano, H. Chikaraishi, S. Imagawa, T. Muroga, N. Noda, N. Ohyabu, T. Satow, J.F. Wang, K.Y. Watanabe, J. Yamamoto , H. Yamanishi, A. Kohyama, H. Matsui, O. Mitarai, T. Noda, A.A. Shishkin, S. Tanaka and T. Terai
Design Assessment of Heliotron Reactor; Sep. 1996 (IAEA-CN-64/G1-5)

NIFS-448 M. Ozaki, T. Sato and the Complexity Simulation Group,
Interactions of Convecting Magnetic Loops and Arcades; Sep. 1996

NIFS-449 T. Aoki,
Interpolated Differential Operator (IDO) Scheme for Solving Partial Differential Equations; Sep. 1996

NIFS-450 D. Biskamp and T. Sato,
Partial Reconnection in the Sawtooth Collapse; Sep. 1996

NIFS-451 J. Li, X. Gong, L. Luo, F.X. Yin, N. Noda, B. Wan, W. Xu, X. Gao, F. Yin, J.G. Jiang, Z. Wu., J.Y. Zhao, M. Wu, S. Liu and Y. Han,
Effects of High Z Probe on Plasma Behavior in HT-6M Tokamak; Sep. 1996

NIFS-452 N. Nakajima, K. Ichiguchi, M. Okamoto and R.L. Dewar,
Ballooning Modes in Heliotrons/Torsatrons; Sep. 1996 (IAEA-CN-64/D3-6)

NIFS-453 A. Iiyoshi,
Overview of Helical Systems; Sep. 1996 (IAEA-CN-64/O1-7)

NIFS-454 S. Saito, Y. Nomura, K. Hirose and Y.H. Ichikawa,
Separatrix Reconnection and Periodic Orbit Annihilation in the Harper Map; Oct. 1996

NIFS-455 K. Ichiguchi, N. Nakajima and M. Okamoto,
Topics on MHD Equilibrium and Stability in Heliotron / Torsatron; Oct. 1996